Hindawi
Journal of Sensors
Volume 2022, Article ID 3142637, 6 pages
https://doi.org/10.1155/2022/3142637

Research Article

Shape Reconstruction of Eccentric Defect in Cylindrical Component by Modified Born Approximation Method

Gangfeng Zheng,[1] **Ze Li**,[1] **Songfeng Liu**,[1] **Hao Dong**,[1] **Bin Wu**,[2] **and Cunfu He**[2]

[1]*School of Materials Science and Engineering, Anhui University of Science and Technology, Huainan 232001, China*
[2]*College of Mechanical Engineering and Applied Electronics Technology, Beijing University of Technology, Beijing 100022, China*

Correspondence should be addressed to Gangfeng Zheng; 649811739@qq.com

Received 7 March 2022; Accepted 29 April 2022; Published 17 May 2022

Academic Editor: Nan Li

In this paper, a cylindrical aluminum sample with an eccentric circular hole was prepared, and ultrasonic measurements were carried out by experimental means. The measurement area was limited to a plane edge perpendicular to the axis of the cylindrical component. The measured waveform data were input into the formula of approximate correction method, and the section image was obtained by using a modified Born approximation (MBA) method. Then, the three-dimensional (3D) shape of the defects in the aluminum sample was reconstructed by superimposing the cross-sectional images. Results showed that the defect reconstruction effect of the two-dimensional section and the 3D defect reconstruction effect were significantly improved by the MBA method.

1. Introduction

Nondestructive testing (NDT) and characterization of defects, such as cracks and voids, are important in many branches of industries [1–4]. Examples are the new types of bridges, grid structures, high-rise buildings, and aerospace crafts. The quality of the component directly affects the equipment performance and service life. Thus, NDT technology is continuously refined [5–9]. NDT of cylindrical components is essential. Cylindrical components have wide applications and considerable market potential. For several aperture geometries, exact inversion formulas can be derived under the assumption that scattering is sufficiently weak for Born approximation (BA) [10–13] to hold and that only backscattering is observed. The solution to this problem does not require far-field approximations. This condition is significant because the classical Born inversion procedure, which is perhaps the simplest and best-known embodiment of the inverse scattering problem, relies crucially on a far-field assumption.

Suitably dealing with the defect echo signal will greatly benefit the quantitative inversion of the defects of cylindrical components [14]. The task of deriving the structure of an object from scattered radiation is known as the inverse scattering problem. The inversion procedure acquires sufficient independent data to reconstruct the scattering parameter by varying the frequency and/or direction of illumination (or object orientation with respect to the source) while measuring the scattered waves over an aperture located beyond the scattering region [15]. If the measurements are performed on a far field with respect to the scattering region, and if the BA is applicable, then the scattering amplitude distribution and the measured time-domain data bear a simple Fourier transform relationship. However, the defect image is distorted when the defect inside the cylindrical component is inverted using the BA method. Therefore, based on the BA method for defect inversion, this paper proposes a quantitative inversion study of defects in cylindrical components using the backscatter echo amplitude correction method for the backscatter echo amplitudes corresponding to different integral wave numbers.

2. Modified Born Approximation (MBA) Method

2.1. Amplitude Correction Technique

2.1.1. Acoustic Pressure of the Probe Emission Sound Field. The application of the BA method is based on the condition that the incident wave is a plane wave. Therefore, as long as the vertical distance between the probe and defect is unchanged, the energy of the incident wave can be consistent, and the ideal result of defect reconstruction can be obtained. However, when the plane nonfocus probe is used to carry out the experimental research, the sound energy will attenuate with the propagation of sound waves in the measured medium due to the divergence of the sound beam emitted by the probe. At the same time, when the defect deviates from the center of the sound beam, its incident energy will change, affecting the amplitude of the backscattered echo signal (Figure 1). The acoustic pressure variation of the probe emission sound field $p(\vec{r}, \omega)$ in space must therefore be studied to accurately correct the backscatter echo amplitude A_m. Here, r is the distance between the source and field points, and ω is the angular frequency.

The probe crystal sheet is discretized into a series of point sources, and the response of the point sound source can be represented by Green's formula function, which can be substituted into the Helmholtz equation.

$$\nabla^2 G(r, \omega) + k^2 G(r, \omega) = -4\pi\delta(r), \tag{1}$$

where $\delta(r)$ denotes the Dirac pulse function and k is the wave number. In accordance with the Kirchhoff boundary integral equation, only the sound field of the point source is required, and the scattered sound field produced by any sound source can be written as follows:

$$p\left(\vec{r}, \omega\right) = \iint_S \left[G\left(\vec{r}, \omega\right) \frac{\partial p_0}{\partial n} - p_0 \frac{\partial G\left(\vec{r}, \omega\right)}{\partial n} \right] dS, \tag{2}$$

where r denotes the distance between the source and field points, dS denotes the discrete elements of the transducer surface, and n is the normal vector of the transducer surface. p_0 denotes the acoustic pressure on the transducer surface. Green's formula for the sound source at the point in free space can be expressed as follows:

$$G\left(\vec{r}, \omega\right) = \frac{1}{4\pi} \frac{\exp\left(-ik_L r\right)}{r}, \tag{3}$$

where k_L is the longitudinal wave number and i is the imaginary unit, $i2 = -1$.

$$p_0 = \rho c_L v_n, \tag{4}$$

where $v_n = e^{\mathrm{ikr}}$ is the surface vibration velocity of the probe crystal sheet, c_L is the longitudinal velocity, and ρ is the medium density.

On the boundary, the partial derivative of the sound pressure is calculated in the normal direction:

$$\frac{\partial p_0}{\partial n} = \rho c_L \left(ike^{\mathrm{ikr}} \right) \cos\left(r, n\right) = i\omega\rho v_n \cos\left(r, n\right). \tag{5}$$

Given that the surface vibration direction and normal angle of the probe crystal sheet are zero, $\cos(r, n) = 1$:

$$\frac{\partial p_0}{\partial n} = i\omega\rho v_n,$$
$$\frac{\partial G\left(\vec{r}, \omega\right)}{\partial n} = \left[\frac{-ik_L \exp\left(-ik_L \vec{r}\right)}{\vec{r}} - \frac{\exp\left(-ik_L \vec{r}\right)}{\vec{r}^{\,2}} \right] \cos\left(r, n\right). \tag{6}$$

In the remote area, $r >> \lambda$, the normal derivative of Green's function can be approximated as follows:

$$\frac{\partial G\left(\vec{r}, \omega\right)}{\partial n} = \frac{-ik_L \exp\left(-ik_L \vec{r}\right)}{\vec{r}},$$

$$\begin{aligned} p\left(\vec{r}, \omega\right) &= \iint \left[\mathrm{G}\left(\vec{r}, \omega\right) \frac{\partial p_0}{\partial n} - p_0 \frac{\partial G\left(\vec{r}, \omega\right)}{\partial n} \right] dS \\ &= \frac{1}{4\pi} \iint \left[\frac{\exp\left(-ik_L \vec{r}\right)}{\vec{r}} i\omega\rho \mathrm{v}_n - \rho \mathrm{c}_L \mathrm{v}_n (-ik_L) \frac{\exp\left(-ik_L \vec{r}\right)}{\vec{r}} \right] dS \\ &= \frac{1}{2\pi} \iint i\omega\rho \mathrm{v}_n \frac{\exp\left(-ik_L \vec{r}\right)}{\vec{r}} dS. \end{aligned} \tag{7}$$

2.2. Amplitude Correction Method. The ultrasonic used in the experiment has a certain bandwidth, and the calculation model $p(\vec{r}, \omega)$ of sound field distribution is based on a single frequency. Therefore, the sound field distribution values at different frequencies in a series of bandwidth ranges must be calculated based on the probe bandwidth. By contrast, the reconstruction model should be used for integration. According to the backscattered echo amplitude $A_m(k_L)$ corresponding to different integral wave numbers k_L, the correction coefficient composed of the sound field model $p(\vec{r}, \omega)$ of the corresponding frequency is used to correct the amplitude.

The concrete implementation process assumes that the crossing time of the probe to the center of the measured component is t_0 (which can be obtained by using the reference component measurement) and an eccentric circular hole defect exists in the measured component. As shown in Figure 2, when the probe is measured at position θ_1, and the signal transit time is $t_1 > t_0$, the defect incident signal sound pressure value $p_1(k_L)$ is less than the component center position sound pressure value $p_0(k_L)$; that is, $p_1(k_L) < p_0(k_L)$. Given the weak incident energy, the amplitude $A_m(k_L, \theta_1)$ of the backscatter echo measured is small. Thus, the ratio of the incident sound pressure p_1 to the sound

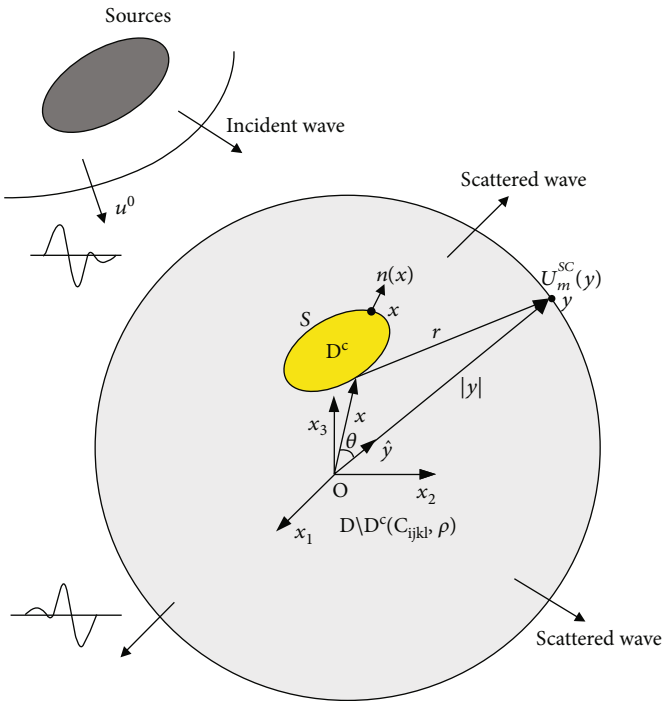

Figure 1: Incident waves scattered from a finite volume D^C in an infinite region.

pressure p_0 at the center of the component should be used as the correction coefficient to correct the amplitude $A_m(k_L, \theta_1)$ of the backscatter echo, as shown in

$$\tilde{A}_m(k_L, \theta_1) = \frac{A_m(k_L, \theta_1)}{(p_1(k_L)/p_0(k_L))} \cdots \quad (8)$$

At different frequencies ω (wave numberk_L), the resulting sound fields vary, and the corresponding $p_0(k_L)$ is different from $p_1(k_L)$. Therefore, the sound field distribution map at different frequencies must be obtained by calculation, followed by the construction of the sound field matrix. In this way, thus, the position of the defect in the sound field can be assessed by time t of defect signal transition, and the sound pressure value $p_n(k_L)$ (similar to the look-up table method) at different frequencies ω (wave number k_L) of the position can be obtained.

In the same way, as shown in Figure 3, when the probe is measured in position θ_2, and the signal transit time is $t_2 < t_0$, the defect incident signal sound pressure value p_2 is larger than the sound pressure value p_0 of the central position of the component; that is, $p_2 > p_0$. The backscatter echo amplitude $A_m(k_L, \theta_2)$ is also measured. Given that the incident energy is relatively strong, and $A_m(k_L, \theta_2)$ is large, the ratio of the incident sound pressure p_2 to the sound pressure p_0 at the center position of the component must be used as

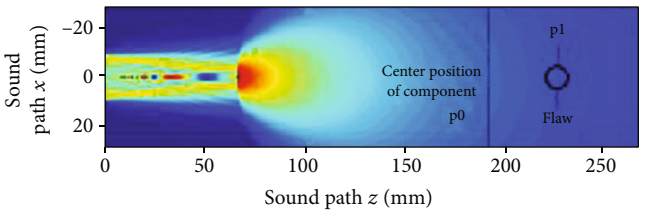

Figure 2: Relative position of probe and eccentric circular hole defect ($t_1 > t_0$).

the correction coefficient to correct the amplitude of the backscattering echo $A_m(k_L, \theta_2)$, as shown in

$$\tilde{A}_m(k_L, \theta_2) = \frac{A_m(k_L, \theta_2)}{(p_2(k_L)/p_0(k_L))} \cdots \quad (9)$$

2.3. MBA Method. The BA method is a low-frequency approximation method sensitive to bulk defects and insensitive to crack defects. Based on the BA method, the backscatter echo amplitude in the theoretical formula of the BA method is corrected. The corrected method is known as the MBA method.

The formula for reconstructing defects is given in [16] by BA methods.

$$\Gamma(x) = \frac{1}{(2\pi)^3} \int_0^{2\pi} \int_0^{\pi} \int_0^{\infty} \frac{\hat{y}_m}{2u^0 k_L^2} A_m(k_L, \theta, \varphi) e^{2ik_L(x_1 \sin\theta \cos\varphi + x_2 \sin\theta \sin\varphi + x_3 \cos\varphi)} 8k_L^2 \sin\theta dk_L d\theta d\varphi. \quad (10)$$

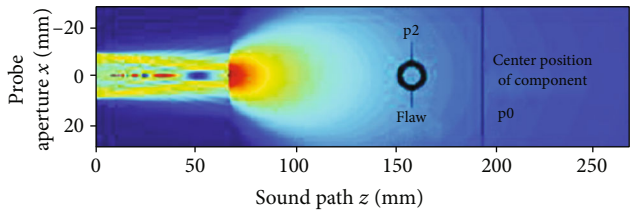

Figure 3: Relative position of the probe and eccentric circular hole defect ($t_2 < t_0$).

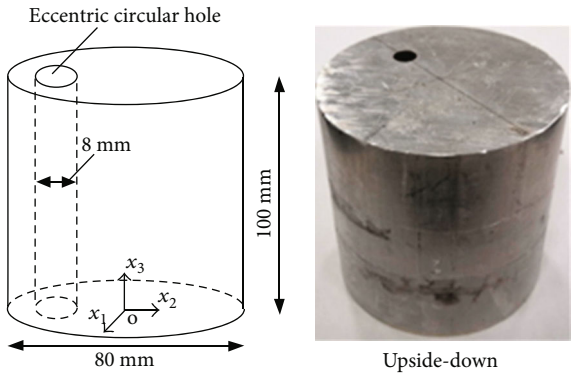

Figure 4: Cylindrical aluminum specimen with eccentric circular hole.

Figure 5: Ultrasonic testing equipment.

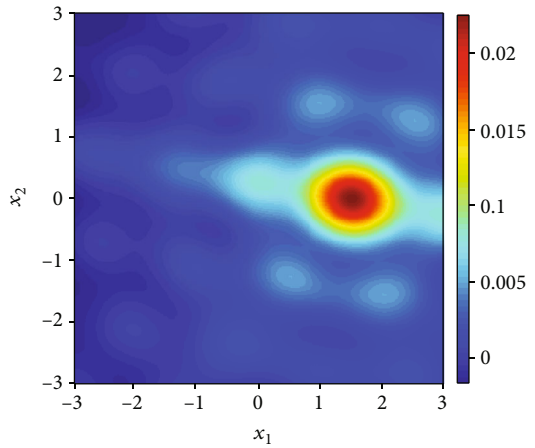

Figure 6: Reconstruction of two-dimensional (2D) section defect before amplitude correction.

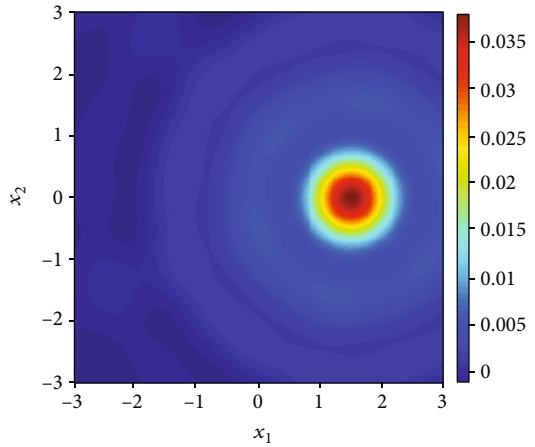

Figure 7: Reconstruction of 2D section defect after amplitude correction.

On this basis, the backscattering echo amplitude in the formula is corrected. After correction, the backscattering echo amplitude becomes $\tilde{A}_m(k_L, \theta)$. Thus, the theoretical formula about the MBA method is obtained as follows:

$$\tilde{\Gamma}(x) = \frac{1}{(2\pi)^3} \int_0^{2\pi} \int_0^{\pi} \int_0^{\infty} \frac{\hat{y}_m}{2u^0 k_L^2} \tilde{A}_m(k_L, \theta, \varphi) e^{2ik_L(x_1 \sin\theta \cos\varphi + x_2 \sin\theta \sin\varphi + x_3 \cos\varphi)} 8k_L^2 \sin\theta dk_L d\theta d\varphi, \quad (11)$$

where

$$\tilde{A}_m(k_L, \theta) = \frac{A_m(k_L, \theta)}{(p(k_L)/p_0(k_L))}. \quad (12)$$

2.4. Experimental Measurements. An aluminum specimen with a diameter of 80 mm was prepared (Figure 4). The specimen includes a cylindrical eccentric circular hole (diameter: 8 mm) as a defect model. Figure 5 shows the experimental setup. The scattered wave from the defect model was measured by the longitudinal–longitudinal pulse-echo method. A contact type transducer with a diameter of 0.125 is moved to the surface of the specimen 10°, a step in the x_1–x_2 plane, and 10 mm, a step in the x_3 direction from $x_3 = 0$ mm to 100 mm.

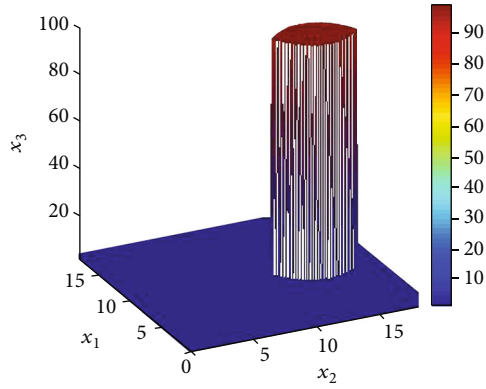

Figure 8: Reconstruction of three-dimensional (3D) defect before amplitude correction (unit: mm).

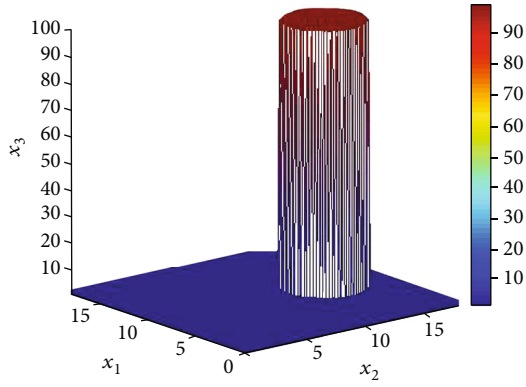

Figure 9: Reconstruction of 3D defect after amplitude correction (unit: mm).

An industrial-specific ultrasonic coupling agent was used as the couplant, resulting in good acoustic coupling and fixation of the transducer. The transducer was driven by a 300 V square wave pulser–receiver. A digital oscilloscope and PC were used for data processing and shape reconstruction. The center frequency of the transducer was 10 MHz, and frequencies ranging from 7.5 MHz to 12.5 MHz were used for defect inversion.

Figures 6 and 7 display the cross-sectional defect images obtained from $\Gamma(x)$ and $\widetilde{\Gamma}(x)$ for the eccentric circular hole, respectively. Given that we collected the data of the scattering amplitudes 10° a step on the surface of the specimen in the x_1–x_2 plane, each cross-sectional defect image was reconstructed by looping 36 times around a cross section. The type of data we processed is a Microsoft Office Excel Worksheet (.xlsx). Figures 6 and 7 show the results of shape reconstruction of BA and MBA, respectively. Total cross-sectional images were piled up, and 3D shape reconstruction was performed by introducing the interpolation for the piled-up cross-sectional images. Figures 8 and 9 reveal the results of 3D shape reconstructions of BA and MBA, respectively.

Figures 7 and 9 show the results after introducing the defect echo amplitude correction coefficient. After the defect amplitude correction, the reconstruction effects of 2D and 3D defects were significantly improved.

3. Conclusions

An MBA method for an eccentric defect in a cylindrical component was presented, and it can relate the backscattering signal distributed on the frequency domain to the geometrical information of defects. Therefore, shape reconstruction can be treated as an inverse problem. The ultrasonic field was calculated in a homogeneous and isotropic aluminum medium after its passage through a curved interface, which was used to correct the amplitude of pulse echoes. The reconstruction qualities before and after compensation were compared, and the results showed that the reconstruction effect can be improved effectively after compensation. We find the following:

(1) The MBA method was proposed.

(2) The shape of the eccentric void defect was reconstructed by the MBA method.

(3) The results showed that the defect reconstruction effect of the 2D section and the 3D defect reconstruction effect were significantly improved by the MBA method.

Data Availability

We confirm that the data supporting the findings of this study are available within the article [and/or] its supplementary materials. Supplementary material file shows the echo data of the first measurement point of the first cross section, and the data format of the other measurement points is the same as that of supplementary material file.

Conflicts of Interest

We declare that there is no conflict of interest regarding the publication of this paper.

Acknowledgments

This work was supported by the National Natural Science Foundation of China (Grant Nos. 51374015 and 10872001), the Key Scientific and Technological Research Project of the Ministry of Education (Grant No. 211076), and the Anhui Fund Project for Outstanding Youths (Grant No. 10040606Y26).

Supplementary Materials

Supplementary material file shows the echo data of the first measurement point of the first cross section, and the data format of the other measurement points is the same as that of the supplementary material file. The supplementary material file corresponds to line 187 in the manuscript. *(Supplementary Materials)*

References

[1] X. F. Guan, J. J. He, and E. M. Rasselkorde, "A time-domain synthetic aperture ultrasound imaging method for material flaw quantification with validations on small-scale artificial and natural flaws," *Ultrasonics*, vol. 56, pp. 487–496, 2015.

[2] Q. I. Jinhao, T. A. Chongcong, J. I. Hongli, Z. H. Chao, and Z. H. Jinling, "Damage detection and material property reconstruction of composite laminates using laser ultrasonic technique," *Transactions of Nanjing University of Aeronautics and Astronautics*, vol. 36, no. 1, pp. 1–11, 2019.

[3] V. F. Maria and F. Zheng, "Sizing of flaws using ultrasonic bulk wave testing: a review," *Ultrasonics*, vol. 88, pp. 26–42, 2018.

[4] J. Rodríguez-Sendra, N. Jiménez, R. Picó, J. Faus, and F. Camarena, "Monitoring the setting of calcium sulfate bone-graft substitute using ultrasonic backscattering," *IEEE Transactions on Ultrasoncs, Ferroelectrics, and Frequency Control*, vol. 66, no. 10, pp. 1658–1666, 2019.

[5] A. Praveen, K. Vijayarekha, S. T. Abraham, and B. Venkatraman, "Signal quality enhancement using higher order wavelets for ultrasonic TOFD signals from austenitic stainless steel welds," *Ultrasonics*, vol. 53, no. 7, pp. 1288–1292, 2013.

[6] A. Raza, W. Hassan, T. Ogay, I. Hwang, and S. Jeon, "Perceptually correct haptic rendering in mid-air using ultrasound phased array," *IEEE Transactions on Industrial Electronics*, vol. 67, no. 1, pp. 736–745, 2020.

[7] H. Abral, V. Lawrensius, D. Handayani, and E. Sugiarti, "Preparation of nano-sized particles from bacterial cellulose using ultrasonication and their characterization," *Carbohydrate Polymers*, vol. 191, pp. 161–167, 2018.

[8] G. Bunget, B. Tilmon, A. Yee et al., "Novel approach of wavelet analysis for nonlinear ultrasonic measurements and fatigue," *Review of Quantitative Nondestructive Evaluation*, vol. 37, pp. 1–10, 2018.

[9] H. Yamada, J. Yotsuji, and K. Ikushima, "Phase-sensitive detection of acoustically stimulated electromagnetic response in steel," *Japanese Journal of Applied Physics*, vol. 57, no. 7S1, p. 07LB09, 2018.

[10] P. Zhang and S. Z. Wang, "Fast prediction of scattered sound field based on Fourier diffraction theory under second-order Born approximation," *Acoustical Physics*, vol. 60, no. 4, pp. 379–386, 2014.

[11] M. Yamada and H. Miyakoshi, "Flow shape reconstruction by three-dimensional linearized inverse scattering method," *Review of Quantitative Nondestructive Evaluation*, vol. 25, pp. 752–759, 2006.

[12] M. Yamada, K. Murakami, K. Nakahata, and M. Kitaharata, "Three dimensional Born and Kirchhoff inversions for shape reconstruction of defects," *Review of Quantitative Nondestructive Evaluation*, vol. 22, pp. 734–741, 2003.

[13] G. F. Zheng, B. Wu, and C. F. He, "Shape reconstruction of mixed type void flaws using Born inversion method," *Measurement*, vol. 46, pp. 3136–3142, 2013.

[14] H. Jin, E. Wu, Y. Han, K. Yang, and J. Chen, "Frequency domain synthetic aperture focusing technique for variable-diameter cylindrical components," *Journal of the Acoustical Society of America*, vol. 142, no. 3, pp. 1554–1562, 2017.

[15] W. Kerr, P. Rowe, and S. G. Pierce, "Accurate 3D reconstruction of bony surfaces using ultrasonic synthetic aperture techniques for robotic knee arthroplasty," *Computerized Medical Imaging and Graphics*, vol. 58, pp. 23–32, 2017.

[16] G. F. Zheng, B. Wu, and C. F. He, "Shape reconstruction of three-dimensional flaw from backscattering data," *Measurement*, vol. 40, no. 9-10, pp. 854–859, 2007.